Dynamical Jahn-Teller effect in a spin-orbital coupled system

Joji Nasu and Sumio Ishihara
Department of Physics, Tohoku University, Sendai 980-8578, Japan
(Received 2 September 2012; published 6 September 2013)

Dynamical Jahn-Teller (DJT) effect in a spin-orbital coupled system on a honeycomb lattice is examined, motivated from recently observed spin-liquid behavior in $Ba_3CuSb_2O_9$. An effective vibronic Hamiltonian, where the superexchange interaction and the DJT effect are taken into account, is derived. We find that the DJT effect induces a spin-orbital resonant state where local spin-singlet states and parallel orbital configurations are entangled with each other. This spin-orbital resonant state is realized in between an orbital-ordered state, where spin-singlet pairs are localized, and an antiferromagnetic ordered state. Based on the theoretical results, a possible scenario for $Ba_3CuSb_2O_9$ is proposed.

DOI: 10.1103/PhysRevB.88.094408 PACS number(s): 75.25.Dk, 75.30.Et, 75.47.Lx

I. INTRODUCTION

No signs for long-range magnetic ordering down to the low temperatures, termed the quantum spin-liquid (QSL) state, are one of the fascinating states of matter in modern condensed matter physics.[1] A number of efforts have been made to realize the QSL states theoretically and experimentally. One prototypical example is the well-known one-dimensional antiferromagnets in which large quantum fluctuation destroys the long-range spin order even at zero temperature and realizes a spin-singlet state without any symmetry breakings. Another candidate for the QSL states has long been searched for in frustrated magnets. An organic salt κ-(BEDT-TTF)$_2$Cu$_2$(CN)$_3$ with a triangular lattice[2] and an inorganic herbertsmithite $ZnCu_3(OH)_6Cl_2$ with a kagome lattice[3] are some examples. Several theoretical scenarios for realization of the QSL, such as Z_2 spin liquid,[4] spin-nematic state,[5] spinon deconfinement,[6] and so on, have been proposed so far.

A transition-metal oxide of our present interest is a new candidate of the QSL state, $Ba_3CuSb_2O_9$, in which $S = 1/2$ spins in Cu^{2+} ions are responsible for the magnetism.[7,8] There are no signs of magnetic orderings down to a few hundred mK, in spite of the effective exchange interactions of 30–50 K. Temperature dependencies of the magnetic susceptibility and the electronic specific heat are decomposed into the gapped component and the low-energy component; the latter is attributed to the so-called orphan spins.[8] It was believed that the QSL behavior originates from the magnetic frustration in a Cu^{2+} triangular lattice. Recent detailed crystal-structural analyses reveal that Cu ions are regularly replaced by Sb ions, and form a short-range honeycomb lattice.[8] One characteristic in the present QSL system is that there is the orbital degree of freedom; twofold orbital degeneracy in Cu^{2+} is suggested by the threefold rotational symmetry around a Cu^{2+}. Almost isotropic g factors observed in the electron-spin resonance (ESR) provide a possibility of no static long-range orbital orders and novel roles of orbital on the QSL.

In this paper, motivated from the recent experiments in $Ba_3CuSb_2O_9$, we examine a possibility of the QSL state in a honeycomb-lattice spin-orbital (SO) system. Beyond the previous theories for QSL in quantum magnets with the orbital degree of freedom,[9–14] the present study focuses on the dynamical Jahn-Teller (DJT) effect, which brings about a quantum tunneling between stable orbital-lattice states. This is feasible in the crystal lattice of $Ba_3CuSb_2O_9$, where O_6 octahedra surrounding Cu^{2+} are separated from each other, unlike the perovskite lattice where nearest-neighboring (NN) two octahedra share an O^{2-}. The SO superexchange (SE) interactions between the separated NN Cu^{2+} are comparable with the vibronic interactions, and a new state of matter is expected as a result of the cooperation between the on-site Jahn-Teller (JT) and intersite SE interactions. We derive the low-energy electron-lattice model where the SE interaction, the JT effect, and the lattice dynamics are taken into account. It is discovered that a spin-orbital resonant state (SORS), where the two degrees of freedom are entangled with each other, is induced by the DJT effect. We examine connections of the quantum resonant state to the long-range ordered states, and provide a possible scenario for $Ba_3CuSb_2O_9$.

In Sec. II, a model Hamiltonian for a spin-orbital-lattice coupled system and calculation methods are introduced. In Sec. III, numerical results are presented. Section IV is devoted to a discussion and summary.

II. MODEL AND METHOD

First we set up the model which consists of the SE interactions between the Cu ions in a honeycomb lattice, and the local vibronic coupling between the Cu d orbitals and O_6 octahedron. The Hamiltonian is given by $\mathcal{H} = \mathcal{H}_{\rm exch} + \mathcal{H}_{\rm JT}$. In the first term for the SE interactions, the doubly degenerate $3d_{3z^2-r^2}$ and $3d_{x^2-y^2}$ orbitals are introduced at each site. The SE interactions are derived from the extended dp-type Hamiltonian where the $3d$ orbitals for a Cu ion and $2p$ orbitals for a O ion are introduced, and the on-site electron-electron interactions and the Cu-O and O-O electron transfers are considered. All possible exchange paths between the NN Cu pairs are taken into account. Details are given in the Supplemental Material (SM).[15] The obtained Kugel-Khomskii-type SO coupled Hamiltonian is given by

$$\begin{aligned}\mathcal{H}_{\rm exch} = J_{\rm SE}\sum_{\langle ij\rangle_l}\big[&\boldsymbol{S}_i\cdot\boldsymbol{S}_j + \bar{J}_{\tau\tau}\tau_i^l\tau_j^l + \bar{J}_{\bar\tau\bar\tau}\bar\tau_i^l\bar\tau_j^l + \bar{J}_{yy}T_i^yT_j^y\\ &+\bar{J}_{ss\tau}\boldsymbol{S}_i\cdot\boldsymbol{S}_j\left(\tau_i^l+\tau_j^l\right) + \bar{J}_{ss\tau\tau}\boldsymbol{S}_i\cdot\boldsymbol{S}_j\tau_i^l\tau_j^l\\ &+\bar{J}_{ss\bar\tau\bar\tau}\boldsymbol{S}_i\cdot\boldsymbol{S}_j\bar\tau_i^l\bar\tau_j^l + \bar{J}_{ssyy}\boldsymbol{S}_i\cdot\boldsymbol{S}_jT_i^yT_j^y\big],\end{aligned}\tag{1}$$

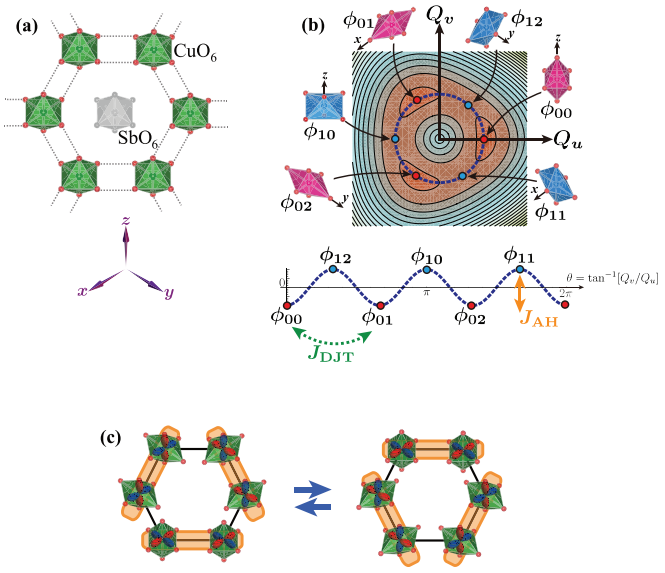

FIG. 1. (Color online) (a) A honeycomb lattice structure for $Ba_3CuSb_2O_9$ (Ref. 16). (b) A contour map of the lower AP surface on the Q_u-Q_v plane. A blue broken line shows a circle for $\rho = \rho_0$. The lower panel represents the AP along this circle as a function of $\theta = \tan^{-1}[Q_v/Q_u]$. Schematic O_6 distortions at the potential minima and maxima are also shown. (c) A schematic picture for the SORS. Shaded bonds represent the spin-singlet and parallel-orbital bonds.

where NN ij sites along a direction $l(=x,y,z)$ [see Fig. 1(a)[16]] is denoted by $\langle ij\rangle_l$. We introduce the spin operator $\boldsymbol{S}_i$ and the pseudospin (PS) operator $\boldsymbol{T}_i$ for the orbital degree of freedom with amplitudes of 1/2. The eigenstate for $T^z = +1/2\,(-1/2)$ describes a state where the $d_{3z^2-r^2}$ ($d_{x^2-y^2}$) orbital is occupied by a hole. For convenience, we introduce the bond-dependent PS operators defined by

$$\tau_i^l = \cos\left(\frac{2\pi n_l}{3}\right) T_i^z - \sin\left(\frac{2\pi n_l}{3}\right) T_i^x \tag{2}$$

and

$$\bar{\tau}_i^l = \cos\left(\frac{2\pi n_l}{3}\right) T_i^x + \sin\left(\frac{2\pi n_l}{3}\right) T_i^z, \tag{3}$$

where $(n_z,n_x,n_y) = (0,1,2)$. The exchange constants are given by the energy parameters in the dp-type Hamiltonian,[15,17] and are normalized by the representative SE interaction $J_{\rm SE}$, a coefficient of $\boldsymbol{S}_i \cdot \boldsymbol{S}_j$. It is shown that $\mathcal{H}_{\rm exch}$ in NN two sites favors an antiferromagnetic (AFM) and ferrotype orbital configuration in a wide parameter region which includes a parameter set for $Ba_3CuSb_2O_9$.[15,18] This is in contrast to the results of the Kugel-Khomskii-type SO Hamiltonian in a square lattice, where a ferromagnetic and antiferrotype orbital configuration is realized. Among a number of terms in the Hamiltonian, the $\boldsymbol{S}_i \cdot \boldsymbol{S}_i$, $\tau_i\tau_j$, $\boldsymbol{S}_i \cdot \boldsymbol{S}_j\tau_i\tau_j$, and $\bar{\tau}_i\bar{\tau}_j$ terms are essential for the SORS of our main interest.

The second term of the Hamiltonian, $\mathcal{H}_{\rm JT}$, describes the local vibronic coupling in each CuO_6 octahedra. We consider the $e \times E$ JT problem where the degenerate $d_{3z^2-r^2}$ and $d_{x^2-y^2}$ orbitals are coupled with the E-symmetric O_6 vibrations, denoted by Q_u and Q_v. The harmonic vibration, the linear JT coupling, and the anharmonic lattice potential are taken into account. We focus on the low-energy vibronic mode, i.e., the rotational motion in the Q_u-Q_v plane along the bottom in the lower adiabatic potential (AP) plane [see Fig. 1(b)]. The Hamiltonian is a well-known form given by[19–24]

$$\mathcal{H}_{\rm rot} = -\frac{1}{2M\rho_0^2}\frac{\partial^2}{\partial\theta^2} + B\rho_0^3\cos 3\theta, \tag{4}$$

with an oxygen mass M, an amplitude of the distortion ρ_0, an angle $\theta = \tan^{-1}(Q_v/Q_u)$ in the AP, and an anharmonic potential B. This model represents the angle motion under the threefold potential, which takes minima (maxima) at $\theta_{0\nu} = 2\pi\nu/3$ ($\theta_{1\nu} = \pi + 2\pi\nu/3$) with $\nu = (0,1,2)$. These angles correspond to the cigar-type [$(3z^2 - r^2)$-type] and the leaf-type [$(x^2 - y^2)$-type] lattice distortions, respectively, as shown in Fig. 1(b). The low-energy states in $\mathcal{H}_{\rm rot}$ are well described by the six Wannier-type vibronic functions,[25] $|\Phi_{\mu\nu}\rangle$, localized around $\theta_{\mu\nu}$, as shown schematically in the lower panel of Fig. 1(b). Then, the low-energy vibronic Hamiltonian is given by

$$\mathcal{H}_{\rm JT} = \sum_{i\mu=(0,1)} \frac{\sigma_\mu}{2}\left[-J_{\rm AH}\sum_\nu |\Phi_{i\mu\nu}\rangle\langle\Phi_{i\mu\nu}| + J_{\rm DJT}\sum_{\nu\neq\nu'} |\Phi_{i\mu\nu}\rangle\langle\Phi_{i\mu\nu'}|\right], \tag{5}$$

where $(\sigma_0,\sigma_1) = (1,-1)$. The first and second terms describe the potential in the angle space and the tunneling motions, respectively. The energy constants, $J_{\rm AH}$ and $J_{\rm DJT}$, are positive and are of the order of $B\rho_0^3$, and $1/(M\rho_0^2)$, respectively. A condition $J_{\rm DJT}/J_{\rm AH} < 1/2$ is required to reproduce the original energy levels, but we regard $J_{\rm DJT}/J_{\rm AH}(\equiv j_D)$ as a free parameter, for convenience. The lowest energy state is a doublet, corresponding to the clockwise and counterclockwise rotations in the θ space. The so-called vibronic reduction factor proposed by Ham,[26,27] i.e., a reduction of the PS moment due to the DJT effect, is 1/2. The detailed derivation of $\mathcal{H}_{\rm JT}$ is given in the SM.[15]

There are three principal energy parameters in the Hamiltonian: the SE interaction $J_{\rm SE}$, the anharmonic potential $J_{\rm AH}$, and the DJT effect $J_{\rm DJT}$. The magnitude of $J_{\rm SE}$ is about 1–10 meV, which is smaller than the exchange interaction in the high-T_c cuprates because of a large distance between the NN Cu sites. Both the energy scales of $J_{\rm AH}$ and $J_{\rm DJT}$ are 1–30 meV.[28,29] Since the three parameters are in the same order of magnitude, competitions and cooperation among them are realized.

The Hamiltonian is analyzed by the exact-diagonalization (ED) method combined with the mean-field (MF) approximation, and the quantum Monte Carlo simulation (QMC)[30,31] with the MF approximation, termed the ED + MF and the QMC + MF methods, respectively. We introduce mainly the results by the ED + MF method. The MF-type decouplings are introduced in the exchange interactions which act on the edge sites of clusters. The Hamiltonian for a six-site cluster under the MFs is diagonalized by the Lanczos algorithm, and the MFs are determined consistently with the states inside of the cluster. This method is equivalent to the hierarchical mean-field method[32,33] where the no long-range ordered phase obtained by the large cluster size[34,35] is reproduced. The adopted parameter values are $J_{\rm SE}/J_{\rm AH} = 0.15$ and are given in Ref. 15. Amplitude of the DJT effect, i.e., $j_D = J_{\rm DJT}/J_{\rm AH}$,

is varied. We find that the obtained results do not depend qualitatively on the parameter J_{SE}/J_{AH} between 0.075 and 1. The exchange Hamiltonian $\mathcal{H}_{exch}$ is also analyzed by the MF approximation and by the ED method as supplementary calculations.

III. RESULT

Spin and orbital structures are monitored by the staggered spin moment given by

$$\mathcal{M}_s = \frac{1}{6}\sum_i (-1)^i S_i^z, \tag{6}$$

and the two PS moments defined by

$$\mathcal{M}_{\tau+} = -\tfrac{1}{6}\left(\tau_A^z + \tau_B^z + \tau_C^x + \tau_D^x + \tau_E^y + \tau_F^y\right) \tag{7}$$

and

$$\mathcal{M}_{\tau-} = -\tfrac{1}{6}\left(\tau_A^x + \tau_B^y + \tau_C^y + \tau_D^z + \tau_E^z + \tau_F^x\right), \tag{8}$$

where subscripts A–F indicate sites in the cluster [see the inset of Fig. 2(b)]. We note that $\mathcal{M}_{\tau+}$ and $\mathcal{M}_{\tau-}$ take their maxima of 0.5 in the threefold orbital-ordered states shown in Figs. 2(d) and 2(e), respectively. A difference between the two, $\mathcal{M}_{PS} \equiv \langle \mathcal{M}_{\tau+} - \mathcal{M}_{\tau-} \rangle$, is regarded as an amplitude of the symmetry breaking. The numerical results are plotted in Fig. 2(a). There is a critical value of j_D, termed $j_{Dc}(=0.75)$. For $j_D \ll j_{Dc}$, $\mathcal{M}_{\tau+} \sim 0.5$ and $\mathcal{M}_{\tau-} \sim -0.25$, implying a symmetry breaking due to the threefold orbital order shown in Fig. 2(d). This orbital order is also suggested by the analyses of $\mathcal{H}_{exch}$. With increasing j_D, absolute values of $\mathcal{M}_+$ and $\mathcal{M}_-$ are reduced. These reductions are reproduced by the QMC + MF method. Above j_{Dc}, $\langle \mathcal{M}_{\tau+} \rangle = \langle \mathcal{M}_{\tau-} \rangle$, interpreted as a superposition of the two PS configurations.

As for the spin sector, neither a finite staggered moment [see Fig. 2(a)], nor a finite local moment $\langle S_i^z \rangle$ at each site, are obtained in a whole parameter region of j_D. As shown in Fig. 2(b), there are two inequivalent NN spin correlations $\langle \boldsymbol{S}_i \cdot \boldsymbol{S}_j \rangle$ for $j_D < j_{Dc}$: Large values are shown in the bonds where the PSs are parallel with each other. On the other hand, for $j_D > j_{Dc}$, $\langle \boldsymbol{S}_i \cdot \boldsymbol{S}_j \rangle$ for all bonds are equivalent. Spin-dimer correlations defined by $K_{ij;kl} = \langle (\boldsymbol{S}_i \cdot \boldsymbol{S}_j)(\boldsymbol{S}_k \cdot \boldsymbol{S}_l) \rangle$ are also plotted in Fig. 2(b) where $K_{AB;BC}$, $K_{AB;CD}$, and $K_{AB;DE}$ are the bond-correlation functions for the NN bonds, the second-NN bonds, and the third-NN bonds, respectively. The second-NN bond correlation function $K_{AB;CD}$ is the largest in a whole parameter region, and $K_{AB;CD}$ in $j_D < j_{Dc}$ is larger than that in $j_D > j_{Dc}$. The results in $j_D < j_{Dc}$ are interpreted as a valence-bond solid state, where spin-singlet pairs are localized at the bonds, in which the NN PSs are parallel with each other. This SO structure is also confirmed in the analysis by the QMC + MF method. Above j_{Dc}, this classically localized PS state associated with the localized single pairs is changed into a quantum superposition of the PS configurations. The spin-singlet dimers are no longer localized in specific bonds, suggested by a reduction of $K_{AB;CD}$ and enhancements of $K_{AB;BC}$ and $K_{AB;DE}$.

We expect from these data that, above j_{Dc}, the local spin-singlet state and the parallel PS configuration are strongly entangled with each other. This is directly confirmed by the

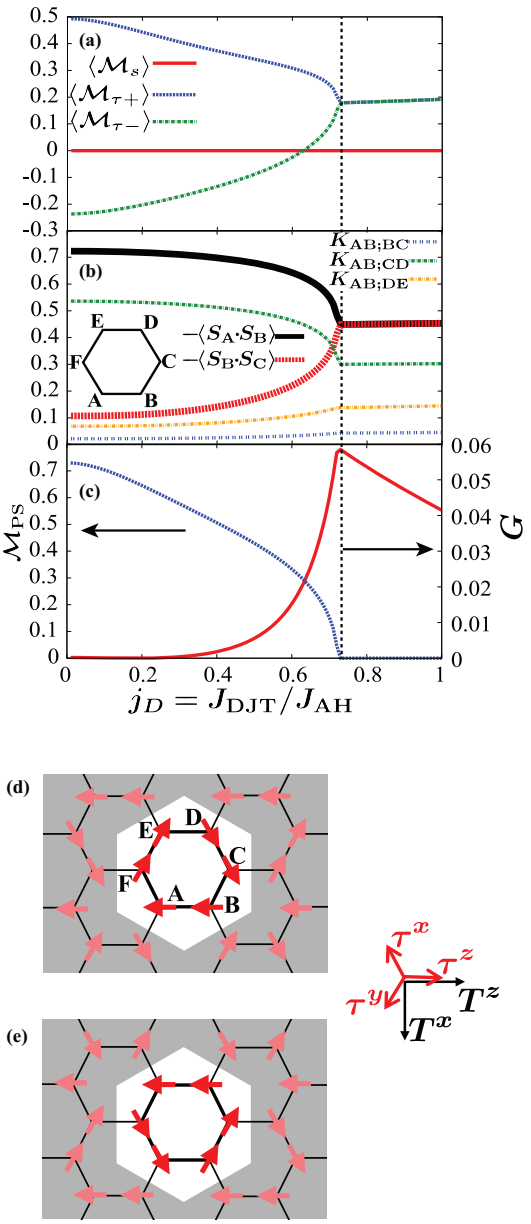

FIG. 2. (Color online) (a) Staggered spin moment $\mathcal{M}_s$, and two PS moments $\mathcal{M}_{\tau+}$ and $\mathcal{M}_{\tau-}$. (b) Spin correlations $\langle \boldsymbol{S}_A \cdot \boldsymbol{S}_B \rangle$ and $\langle \boldsymbol{S}_B \cdot \boldsymbol{S}_C \rangle$ (bold lines), and spin-dimer correlations $K_{AB;BC}$, $K_{AB;CD}$, and $K_{AB;DE}$ (thin lines). The inset shows a six-site cluster. (c) SO correlation function G, and the threefold orbital order parameter $\mathcal{M}_{PS}$. The broken line indicates j_{Dc}. (d), (e) Two kinds of the threefold orbital-ordered states.

SO correlation function defined by[36]

$$G = \left[\frac{1}{6}\sum_{\langle ij \rangle_l} G_{ij}^l\right]^2, \tag{9}$$

with

$$G_{ij}^l = 16\left[\langle (\boldsymbol{S}_i \cdot \boldsymbol{S}_j)(\tau_i^l \tau_j^l) \rangle - \langle \boldsymbol{S}_i \cdot \boldsymbol{S}_j \rangle \langle \tau_i^l \tau_j^l \rangle\right]. \tag{10}$$

The results are presented in Fig. 2(c). Spin and orbital sectors are decoupled at $j_D = 0$, and are strongly entangled near

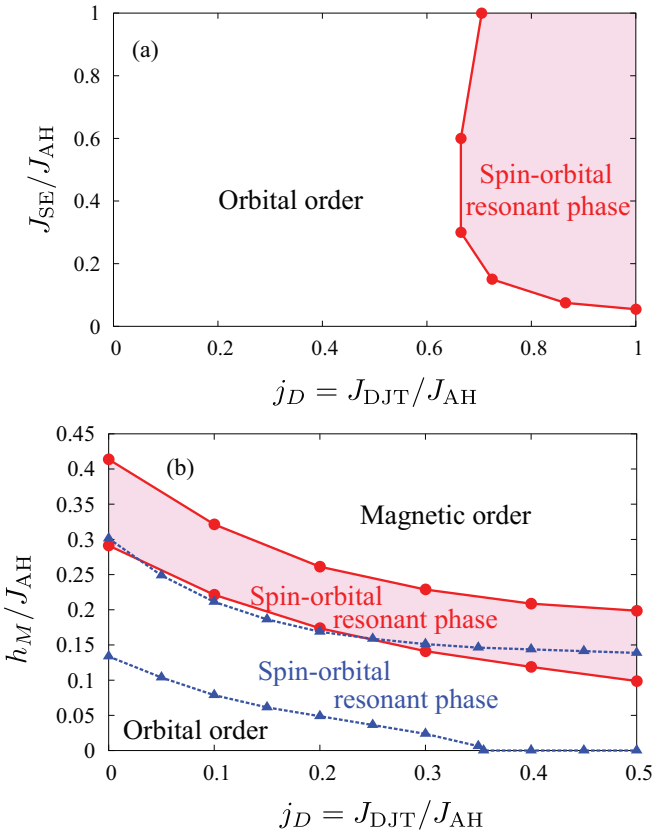

FIG. 3. (Color online) (a) Phase diagram on the plane of $J_{\rm DJT}/J_{\rm AH}$ and $J_{\rm SE}/J_{\rm AH}$. (b) Phase diagram on the plane of $J_{\rm DJT}/J_{\rm AH}$ and $h_M/J_{\rm AH}$. The circles and triangles represent the phase boundaries with and without the interaction between the octahedra, respectively. The parameter of this interaction is chosen to be $K/J_{\rm AH} = 0.1$ [see the details in the SM (Ref. 15)].

and above j_{Dc}. This is consistent with the picture where the spin-singlet state and the parallel PS configuration are realized as a quantum mechanical superposition.[9,11,36] The phase diagram on a plane of $J_{\rm DJT}$-$J_{\rm SE}$ is shown in Fig. 3(a). The SORS diminishes both in the weak and strong $J_{\rm SE}$ limits; that is, the SORS is realized by interplay of $J_{\rm SE}$ and $J_{\rm DJT}$.

To examine a connection of the present SORS to the long-range spin ordered state in the honeycomb-lattice Heisenberg model, we release the orbital degeneracy by applying the artificial external field on the orbital-lattice sector. The is given by

$$\mathcal{H}_M = -h_M \sum_{i\mu\nu\nu'} \sigma_\mu F_{\nu\nu'} |\Phi_{i\mu\nu}\rangle\langle\Phi_{i\mu\nu'}|, \qquad (11)$$

where $F_{\nu\nu'} = \frac{i}{\sqrt{3}} \sum_l \varepsilon_{l\nu\nu'}$ with the Levi-Civita completely antisymmetric tensor $\varepsilon_{l\nu\nu'}$.[15] The artificial field makes clockwise and counterclockwise rotations in the θ space inequivalent, and lifts the ground-state degeneracy. Then, the Hamiltonian is reduced into the AFM Heisenberg model without the orbital degree of freedom. The phase diagram on a plane of j_D and h_M is shown in Fig. 3(b). It is obtained that the Néel order appears for large h_M. The SORS is realized in between the spin ordered state and the orbital-ordered state which is realized in small j_D and h_M.

So far, each O_6 lattice vibration is assumed to be independent from each other. Here we show that the SORS is realized in more realistic parameter space, when the crystal lattice effect is taken into account. The interactions $\mathcal{H}_{\rm inter}$ between the NN O_6 octahedra are modeled by introducing the spring constant between the NN octahedra K (see details in Ref. 15). As shown in Fig. 3(b), the SORS is shifted to the lower side of j_D and h_M. Without the artificial field ($h_M = 0$), j_{Dc} is decreased down to 0.35. This result satisfies the condition of $j_D < 0.5$, in which $\mathcal{H}_{\rm JT}$ is valid as an effective Hamiltonian for the low-energy vibronic states of $\mathcal{H}_{\rm rot}$.

We have shown that the present SORS emerges under the quantum orbital state. A similar orbital state is known in the honeycomb-lattice "orbital-only" model without the spin degree of freedom, given by

$$\mathcal{H}_{\rm orb} = J \sum_{\langle ij\rangle_l} \tau_i^l \tau_j^l. \qquad (12)$$

Instead of a conventional long-range order, a quantum superposition of the orbital PSs is realized in $\mathcal{H}_{\rm orb}$.[37] Here, we

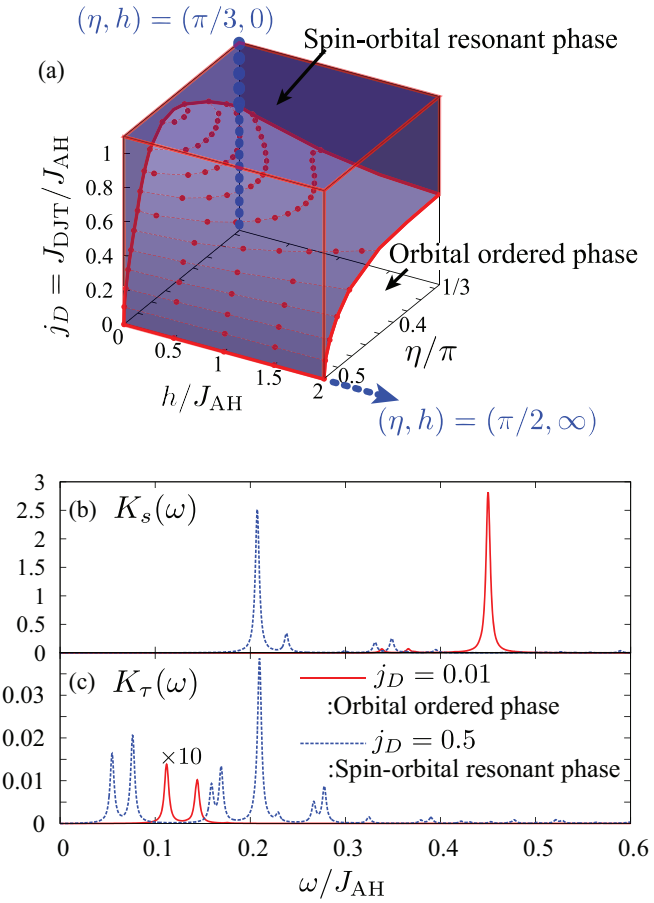

FIG. 4. (Color online) (a) Phase diagram for the model where the generalization of the electron transfer η and the staggered magnetic field h are taken into account (see text). The SE interaction model $\mathcal{H}_{\rm exch}$ and the orbital-only model $\mathcal{H}_{\rm orb}$ correspond to $(\eta,h) = (\pi/3,0)$ and $(\pi/2,\infty)$, respectively. A shaded area shows the SO resonant phase. (b) The dynamical spin-correlation function $K_s(\omega)$, and (c) the dynamical orbital-correlation function $K_\tau(\omega)$ in the orbital-ordered phase ($j_D = 0.01$) and in the SO resonant phase ($j_D = 0.5$). Parameter values are chosen to be the same as those in Fig. 3(b).

connect the present SE Hamiltonian $\mathcal{H}_{\rm exch}$ in Eq. (1) to $\mathcal{H}_{\rm orb}$, and examine a relation between the two orbital states. We generalize the electron transfer as $t_{pd} \to t_{pd}(\eta)$ by introducing a parameter η, and apply the staggered magnetic field as

$$\mathcal{H}_h = -h \sum_i (-1)^i S_i^z. \tag{13}$$

Detailed procedures are explained in the SM.[15] In the (η,h) parameter space, the present model and the orbital-only model are located at $(\eta,h) = (\pi/3,0)$ and $(\pi/2,\infty)$, respectively. In Fig. 4(a), the phase diagram as functions of h, η, and j_D is presented. The SORS at $(\eta,h) = (\pi/3,0)$ and $j_D > j_{Dc} = 0.75$ continuously connects to the orbital resonant state in the orbital-only model realized in $(\eta,h) = (\pi/2, \gg J_{\rm AH})$. This result implies that the present SORS belongs to the same class of the orbital resonance state in the orbital-only model, and supports the physical picture given in Fig. 1(c). It is worth noting that the orbital resonant state in $\mathcal{H}_{\rm orb}$ remains in the infinite size limit.[37] We suppose that the present SORS is survived even in large cluster systems.

IV. DISCUSSION AND SUMMARY

Based on the calculations, we propose a scenario for $Ba_3CuSb_2O_9$.[7,8] The x-ray diffraction experiments suggest a short-range honeycomb-lattice domain of the order of 10 Å, which justifies the present finite-size cluster analyses to mimic the realistic situation. The observed positive Weiss constant is not trivial in conventional orbital-degenerate magnets where the ferromagnetic interaction is dominant,[38] and can be explained by the present calculation where the exchange paths are properly taken into account in a realistic lattice. As for the no long-range SO orders in the hexagonal samples, the present SORS is a plausible candidate. The temperature dependence of the magnetic susceptibility is decomposed into the Curie tail and a gapped component. The former is attributed to the orphan spins, and the latter is explained by the present SORS where the short-range spin singlets are realized. Existence of the gapped magnetic excitation is also suggested by the specific heat, the inelastic neutron scattering, and the nuclear magnetic resonance measurements.[8,39] The time scale for the SO dynamics in SORS is governed by the local DJT effect $J_{\rm DJT} \sim$ 1–10 meV and the intersite exchange interaction $J_{\rm SE} \sim$ 1–10 meV, both of which are in between the ESR time scale ($\sim 10^{-9}$ s) and the x-ray time scale ($\sim 10^{-15}$ s). This fact can explain the contradicted experimental results: the almost isotropic ESR signal and the anisotropic extended x-ray absorption fine structure data,[8] which are in contrast to the conventional strong JT coupling systems.[40,41]

Finally, our theory provides a number of forceful predictions in $Ba_3CuSb_2O_9$ and other materials. There will be a crossover frequency/magnetic field in ESR, corresponding to $J_{\rm DJT}$ and $J_{\rm SE}$, where the anisotropy in the g factor is changed qualitatively. Dynamics of the orbital-lattice coupled vibronic excitation is expected to be observed directly by inelastic light/x-ray scattering spectra around 1–10 meV. A key ingredient in the present SORS is the SO entanglement. To demonstrate the SO entanglement from the viewpoint of dynamics, we show, in Figs. 4(b) and 4(c), the dynamical spin-correlation function $K_s(\omega)$ and the dynamical orbital-correlation function $K_\tau(\omega)$, respectively. We define

$$K_u(\omega) = -\frac{1}{\pi} {\rm Im} \left\langle \mathcal{M}_u \frac{1}{\omega - (\mathcal{H} + \mathcal{H}_{\rm inter}) + E_0 + i\eta} \mathcal{M}_u \right\rangle, \tag{14}$$

where $\mathcal{M}_u = \mathcal{M}_s$ for spin ($u = s$), $\mathcal{M}_u = \frac{1}{6}\sum_i T_i^z$ for orbital ($u = \tau$), an infinitesimal constant η, and the ground-state energy E_0. Gapped spin excitations and low-lying orbital excitations are seen in SORS and are consistent with the inelastic neutron and x-ray scattering experiments, respectively.[8,42] In SORS ($j_D = 0.5$), in contrast to the orbital-ordered phase ($j_D = 0.01$), an intensive orbital excitation is seen around the lowest spin-excitation energy, where we obtained that the SO correlation function G is much larger than that in the ground state. This SO entangled excitation will be confirmed by combined analyses of the inelastic neutron and x-ray scattering experiments. We also predict that the SORS is suppressed by applying the strong uniaxial pressure which breaks an energy balance between spin and orbital. Finally, in addition to $Ba_3CuSb_2O_9$, the present SORS scenario is applicable to other materials, where octahedra are not shared and JT centers are separated from each other. One plausible candidate is orbital-degenerate magnets in the ordered double-perovskite crystal lattice.

In summary, we find that the SORS is realized by the DJT effect in a honeycomb-lattice SO model. The present study provides systematic explanations for the recent experiments in $Ba_3CuSb_2O_9$. With increasing DJT, the local orbital moments are reduced, and the long-range orbital-ordered state is transferred to the quantum resonant state at the quantum-critical point. This interplay between the local quantum state and the classical order is analogous to the well-known quantum-critical phenomena in the Kondo-lattice model. This theory also proposes a route to the QSL state in orbitally degenerate systems without geometrical frustration.

ACKNOWLEDGMENTS

We thank S. Nakatsuji, H. Sawa, M. Hagiwara, and Y. Wakabayashi for helpful discussions. This work was supported by KAKENHI from MEXT and Tohoku University "Evolution" program. J.N. is supported by the global COE program "Weaving Science Web beyond Particle-Matter Hierarchy" of MEXT, Japan. Parts of the numerical calculations are performed in the supercomputing systems in ISSP, the University of Tokyo.

[1] L. Balents, Nature (London) **464**, 199 (2010).

[2] Y. Shimizu, K. Miyagawa, K. Kanoda, M. Maesato, and G. Saito, Phys. Rev. Lett. **91**, 107001 (2003).

[3] J. S. Helton, K. Matan, M. P. Shores, E. A. Nytko, B. M. Bartlett, Y. Yoshida, Y. Takano, A. Suslov, Y. Qiu, J.-H. Chung, D. G. Nocera, and Y. S. Lee, Phys. Rev. Lett. **98**, 107204 (2007).

[4]N. Read and S. Sachdev, Phys. Rev. Lett. **66**, 1773 (1991).
[5]H. Tsunetsugu and M. Arikawa, J. Phys. Soc. Jpn. **75**, 083701 (2006).
[6]T. Senthil and M. P. A. Fisher, Phys. Rev. B **62**, 7850 (2000).
[7]H. D. Zhou, E. S. Choi, G. Li, L. Balicas, C. R. Wiebe, Y. Qiu, J. R. D. Copley, and J. S. Gardner, Phys. Rev. Lett. **106**, 147204 (2011).
[8]S. Nakatsuji, K. Kuga, K. Kimura, R. Satake, N. Katayama, E. Nishibori, H. Sawa, R. Ishii, M. Hagiwara, F. Bridges, T. U. Ito, W. Higemoto, Y. Karaki, M. Halim, A. A. Nugroho, J. A. Rodriguez-Rivera, M. A. Green, and C. Broholm, Science **336**, 559 (2012).
[9]L. F. Feiner, A. M. Oleś, and J. Zaanen, Phys. Rev. Lett. **78**, 2799 (1997).
[10]G. Khaliullin and V. Oudovenko, Phys. Rev. B **56**, R14243 (1997).
[11]Y. Q. Li, M. Ma, D. N. Shi, and F. C. Zhang, Phys. Rev. Lett. **81**, 3527 (1998).
[12]F. Vernay, K. Penc, P. Fazekas, and F. Mila, Phys. Rev. B **70**, 014428 (2004).
[13]L. Thompson and P. A. Lee, arXiv:1202.5655.
[14]P. Corboz, M. Lajkó, A. M. Läuchli, K. Penc, and F. Mila, Phys. Rev. X **2**, 041013 (2012).
[15]See Supplemental Material at http://link.aps.org/supplemental/10.1103/PhysRevB.88.094408 for detailed formulations.
[16]The axes of coordinate, x,y,z, are chosen to be parallel to the orthogonal Cu-O bond directions in an octahedron. Since the exchange paths are identified by a plane (lm), a NN Cu-Cu bond is labeled by an index n, where (l,m,n) are the cyclic permutations of the Cartesian coordinates.
[17]W. A. Harrison, *Electronic Structure and the Properties of Solids, The Physics of the Chemical Bond* (W. H. Freeman and Company, San Francisco, 1980).
[18]Y. Mizuno, T. Tohyama, S. Maekawa, T. Osafune, N. Motoyama, H. Eisaki, and S. Uchida, Phys. Rev. B **57**, 5326 (1998).
[19]J. S. Koehler and D. M. Dennison, Phys. Rev. **57**, 1006 (1940).
[20]M. C. M. O'Brien, Proc. R. Soc. London, Ser. A **281**, 323 (1964).
[21]J. C. Slonczewski, Solid State Commun. **7**, 519 (1969).
[22]F. I. B. Williams, D. Krapla, and D. Breen, Phys. Rev. **179**, 255 (1969).
[23]R. Engleman, *The Jahn-Teller Effect in Molecules and Crystals* (Wiley, London, 1972).
[24]I. Bersuker, *The Jahn-Teller Effect* (Cambridge University Press, Cambridge, 2006).
[25]B. Halperin and R. Englman, Solid State Commun. **7**, 1579 (1969).
[26]F. Ham, Phys. Rev. **138**, A1727 (1965).
[27]F. Ham, Phys. Rev. **166**, 307 (1968).
[28]P. García-Fernández, A. Trueba, M. T. Barriuso, J. A. Aramburu, and M. Moreno, Phys. Rev. Lett. **104**, 035901 (2010).
[29]T. A. Abtew, Y. Y. Sun, B.-C. Shih, P. Dev, S. B. Zhang, and P. Zhang, Phys. Rev. Lett. **107**, 146403 (2011).
[30]A. F. Albuquerque, F. Alet, P. Corboz, P. Dayal, A. Feiguin, S. Fuchs, L. Gamper, E. Gull, S. Gürtler, A. Honecker, R. Igarashi, M. Körner, A. Kozhevnikov, A. Läuchli, S. R. Manmana, M. Matsumoto, I. P. McCulloch, F. Michel, R. M. Noack, G. Pawowski, L. Pollet, T. Pruschke, U. Schollwöck, S. Todo, S. Trebst, M. Troyer, P. Werner, and S. Wessel, J. Magn. Magn. Mater. **310**, 1187 (2007).
[31]S. Todo and K. Kato, Phys. Rev. Lett. **87**, 047203 (2001).
[32]L. Isaev, G. Ortiz, and J. Dukelsky, Phys. Rev. B **79**, 024409 (2009).
[33]J. Nasu and S. Ishihara, J. Phys. Soc. Jpn. **80**, 033704 (2011).
[34]H.-C. Jiang, H. Yao, and L. Balents, Phys. Rev. B **86**, 024424 (2012).
[35]A. Läuchli, J. C. Domenge, C. Lhuillier, P. Sindzingre, and M. Troyer, Phys. Rev. Lett. **95**, 137206 (2005).
[36]A. M. Oleś, P. Horsch, L. F. Feiner, and G. Khaliullin, Phys. Rev. Lett. **96**, 147205 (2006).
[37]J. Nasu, A. Nagano, M. Naka, and S. Ishihara, Phys. Rev. B **78**, 024416 (2008).
[38]K. Kugel and D. Khomskii, Usp. Fiz. Nauk **136**, 621 (1982) [Sov. Phys. Usp. **25**, 231 (1982)].
[39]J. A. Quilliam, F. Bert, E. Kermarrec, C. Payen, C. Guillot-Deudon, P. Bonville, C. Baines, H. Luetkens, and P. Mendels, Phys. Rev. Lett. **109**, 117203 (2012).
[40]M. C. Sánchez, G. Subías, J. García, and J. Blasco, Phys. Rev. Lett. **90**, 045503 (2003).
[41]J. Deisenhofer, B. I. Kochelaev, E. Shilova, A. M. Balbashov, A. Loidl, and H.-A. Krug von Nidda, Phys. Rev. B **68**, 214427 (2003).
[42]Y. Ishiguro, K. Kimura, S. Nakatsuji, S. Tsutsui, A. Q. R. Baron, T. Kimura, and Y. Wakabayashi, Nat. Commun. **4**, 2022 (2013).